EUROFUSION WPS1-PR(16) 16773

K.J. McCarthy et al.

Plasma Fuelling with Cryogenic Pellets in the stellarator TJ-II

Preprint of Paper to be submitted for publication in
Nuclear Fusion

This work has been carried out within the framework of the EUROfusion Consortium and has received funding from the Euratom research and training programme 2014-2018 under grant agreement No 633053. The views and opinions expressed herein do not necessarily reflect those of the European Commission.

Plasma Fuelling with Cryogenic Pellets in the Stellarator TJ-II

K. J. McCarthy, N. Panadero, J. L. Velasco, J. Hernández Sánchez, R. García, J. M. Fontdecaba, M. Navarro, I. Pastor, A. Soleto and the TJ-II Team

Laboratorio Nacional de Fusión, CIEMAT, Madrid, Spain

author's email: kieran.mccarthy@ciemat.es

Abstract

Cryogenic pellet injection is a widely used technique to deliver fuel to the core of magnetically confined plasmas. Indeed, core fuelling is a critical issue on the pathway to the development of steady-state scenarios in magnetically confined plasma devices, in particular, for helical devices. Recently, a pipe gun type injector was commissioned on the TJ-II, a low magnetic shear stellarator of the heliac type. It can inject up to 4 hydrogen pellets, containing between 3×10^{18} and 4×10^{19} atoms, per discharge at 800 to 1200 m s^{-1} from the low-field side of plasmas created and/or maintained by electron cyclotron resonance and/or neutral beam injection heating in this medium sized device. In this paper, after describing the background and the experimental set-up employed, we report on pellet ablation and fuelling efficiency studies made with both heating methods.

Keywords: Stellarator, pellet, ablation, fuelling, plasma response

1. Introduction

Core fuelling is a critical issue on the pathway to the development of steady-state scenarios in future magnetically confined fusion reactors, in particular, for helical type devices [1, 2]. Indeed, neoclassical theory predicts that, for such devices, on-axis electron cyclotron resonance heating (ECRH) necessitates a particle source situated at the same radial position as the ECRH with an analogous deposition profile shape in order to mitigate potential core particle depletion [3]. Although gas puffing is a well-established tool for creating and

sustaining plasmas in most current tokamaks and stellarators, its location at the plasma edge means that it will become inefficient for very large devices [4, 5]. Furthermore, particle recycling is predicted to be minimal since plasma-wall interactions will predominantly occur in the divertor region. In addition, neutral beam injection (NBI) is also a habitual technique for plasma core fuelling [6]. However, the introduction of such an energy source may become problematic from the point of view of density control, in particular in stellarators, where energy and particle transport are coupled in the core. Indeed, coupling may lead to hollow density profiles (NBI tends to reduce the hollowness of density profiles but the energy source tends to increase it), thereby reinforcing the need for fuelling techniques that avoid such drawbacks [3]. Nonetheless, there exists a prime candidate that permits achieving relatively localized core fuelling without an associated energy source. It is the cryogenic pellet injection, a well-developed technology that has been employed on numerous magnetically confined plasma devices for several decades [7, 8, 9].

Cryogenic pellet injection has been, and continues to be, the subject of intense research. For instance, in the case of stellarators, pellet penetration and fuelling studies performed on the W7-AS showed good agreement between measured and predicted penetration depths and indicated an influence of central electron temperature, $T_e(0)$, on fuelling efficiency [10]. Also, in the Large Helical Device (LHD), a pellet injector extended its operational regime with good energy confinement [11, 12]. More recently, in the TJ-II, where a four-barrel compact injector began operation in 2014 [13], several studies have been performed to date. For instance, one study demonstrates that, for certain operational scenarios, particle diffusive transport can redistribute some of the pellet particles towards the core, thereby compensating for, or slowing down, core depletion [14]. Another reports on the first observation of relaxation of a zonal electrostatic potential perturbation after pellet injection [15] while a third one describes the transient behaviour of impurity transport on a flux surface as triggered by

pellet injection [16]. Finally, it is expected that a pellet injector will become available for the recently inaugurated Wendelstein 7-X during its second phase of operation. Its goal is to undertake, for instance, comparative studies between low- and high-field side injections in order to quantify the influence on penetration and fuelling of possible ∇B-induced E×B polarized drifting of the partly ionized cloud that surrounds an ablating pellet [9, 17].

In this work cryogenic pellet ablation and fuelling studies performed on the stellarator TJ-II are summarized and the main results are reported. For this hydrogen pellets are injected from its low-field side (LFS) into ECRH or NBI-heated plasmas and pellet ablation is followed using silicon diode based light detection systems while the temporal evolution of particles deposited in the plasma is followed using a microwave interferometer and a Thomson scattering diagnostic. With these and with additional diagnostic systems, the influence of plasma parameters, as well as phenomena such as suprathermal electron populations, can be evaluated. Finally, ratios between the number of pellet particles deposited in the plasma and pellet particle content (fuelling efficiency) are determined for a wide range of target plasma densities and temperatures.

2. Background

The ablation process of a cryogenic pellet as it penetrates through magnetically confined plasma has been intensively studied, albeit several aspects remain to be fully understood. For this, models based on Neutral Gas Shielding (NGS) are generally utilized to characterize ablation as a pellet enters the plasma edge and penetrates through to the core [18]. It is considered that plasma electrons impacting on the pellet create a cloud of neutral atoms that subsequently surrounds, and travels along with, the pellet. Heat transfer from background plasma particles then ionizes the ablated fuelling material, which streams out along the magnetic field lines. The surrounding neutral gas cloud subsequently checks the energy flow to the solid. Then, as long as sufficient pellet mass remains to sustain this cloud, the shielding

will be maintained. Finally, once the pellet is fully ablated, the cloud dissipates, the local density quickly equilibrates and pellet material diffuses around the plasma.

It is well known that in tokamaks a rapid outward radial displacement of ablatant occurs during pellet penetration due to a ∇B effect [9]. It is ascribed to a vertical curvature and ∇B drift current induced inside the partially ionized cloud by the radial magnetic field variation, where an uncompensated vertical drift current inside the weakly diamagnetic ablation cloud gives rise to charge separation, and hence an electrostatic field. This induces an E×B drift, with velocity V_d, that may be greater than the pellet velocity, V_p, towards the low-field side (LFS) edge of the plasma where V_p is manifested as a radial displacement, ΔR, between the cloud light emission profile, *e.g.*, Balmer H_α at $\lambda = 656.3$ nm for hydrogen, and the deposited pellet electron profile [19]. As a consequence high-field side (HFS) injection facilitates higher penetration and core fuelling efficiency [20]. However, HFS injection is limited to velocities of a few hundred meters per second in order to ensure pellet survival along bended guide tubes [21]. In contrast, in stellarators, the drift changes direction depending on position along the magnetic field line, and hence the expanding ablation cloud, may not necessarily drift directly outwards [16]. Indeed, the effect of this drift on fuelling may be considered modest when compared with that in tokamaks [22]. As will be seen, the TJ-II is especially suited to study these effects given that it is equipped with a pellet injector and a large number of diagnostic systems. These are outlined next.

3. Experimental set-up

3.1 TJ-II stellarator

The TJ-II is a low magnetic shear stellarator of the heliac type. It has a major radius of 1.5 m and an average minor radius, *a*, of ≤0.22 m [23]. Its magnetic fields are generated by a system of poloidal, toroidal and vertical field coils and the resultant plasma cross-section is bean shaped. Note: at plasma centre, $B_0 \leq 1.1$ T. The device is designed to have a high degree of

magnetic configuration flexibility. During experimental campaigns, plasmas are created using hydrogen, deuterium or helium as the working gas, and are heated using ECRH with one or two gyrotrons operated at 53.2 GHz, *i.e.*, the 2nd harmonic of the electron cyclotron resonance frequency ($P_{ECRH} \leq 500$ kW, $t_{discharge} \leq 300$ ms). With ECRH, central electron densities, $N_e(0)$, and $T_e(0)$ up to 1.7×10^{19} m^{-3} and 1 keV, respectively, can be achieved. Plasmas have also been created and/or maintained by the injection of accelerated neutral hydrogen atoms ($E_{NBI} \leq 34$ keV, $P_{NBI} \leq 0.7$ MW throughput) from two tangential NBI systems. Note: when using NBI heating only, plasmas are generated by employing a single beam and initial toroidal electric fields, induced by increasing coil currents during ramp-up by up to 3.8 V/turn. In both cases, NBI heating results in plasmas with $N_e(0) \leq 5\times10^{19}$ m^{-3} and $T_e(0) \leq 400$ eV when a lithium coating is applied to the vacuum vessel wall [24]. Finally, the majority ion temperature, $T_i(0)$, is ≤ 120 eV for both heating schemes.

In TJ-II discharges, fuelling is normally accomplished using a set of piezoelectric valves distributed toroidally around the vacuum vessel and driven by a pre-programmed voltage signal [25]. The signal profile, defined by the desired density profile, provides both pre-fill and active fuelling before and along a discharge, respectively. The average hydrogen flow rate for each valve is $\leq 3.5\times10^{19}$ particles s^{-1} [26].

3.2 Cryogenic pellet injection

A pellet injector has been operating on the TJ-II since mid-2014 [13]. It is a 4-pellet system, developed in conjunction with the Fusion Energy Division of Oak Ridge National Laboratory, Tennessee, USA. It is equipped with a cryogenic refrigerator for *in-situ* hydrogen pellet formation, fast propellant valves for pellet acceleration (800 to 1200 m/s), in-line diagnostics for determining pellet velocity and mass [27], plus straight delivery lines. See Figure 1. As noted, the injection line is equipped with a light emitting/sensitive diode combination and a microwave resonance cavity. The former provides a timing signal only

while the latter provides a timing signal whose amplitude is mass dependent. For TJ-II, small pellets with 0.42 mm (*Type-1*) and 0.66 mm (*Type*-2) diameters (containing $\leq 4\times10^{18}$ and $\leq 1.2\times10^{19}$ hydrogen atoms, respectively) are required for experiments in which the electron density must not rise above the gyrotron cut-off limit ($\sim 1.7\times10^{19}$ m^{-3}). Note: for the standard configuration the plasma volume contained within the last-closed magnetic surface (LCMS) is ~1.1 m^3. Larger pellets with diameters of 0.76 mm (*Type-3*) and 1 mm (*Type-4*), containing $\leq 1.8\times10^{19}$ and $\leq 4.1\times10^{19}$ hydrogen atoms, respectively, can be injected into higher density NBI-heated plasmas.

A significant advantage of the current set-up is the optical access to the pellet path through the plasma, *i.e*., through viewports located above (TOP) and behind (SIDE) the pellet flight paths. See Figure 1. In order to collect the light emitted by the neutral, or partially ionized, cloud that surrounds an ablating pellet, amplified silicon diodes fitted with interference filters centred at 660 +/- 2 nm, and a fast-frame camera, equipped with a coherent fibre bundle, are located outside these viewports, which together with the broad range of standard diagnostics available provide a powerful diagnostic capability [13]. Note: the SIDE diode is sometimes replaced by an avalanche photodiode (APD). Then, with these diode signals and knowing the pellet velocity and plasma entry time, pellet ablation profiles and penetration lengths can be established. It should be noted that due to the design of the pellet injector (54 mm vertical and horizontal separation between guide tubes), the flight paths for lines 2 and 3 do not cross the plasma centre for the nominal magnetic configuration, rather, their closest approaches are at $\rho = 0.273$ and 0.45, respectively [13], where $\rho = r/a$ is the normalized plasma radius. However, pellet types can be interchanged between injection lines.

3.4 Plasma diagnostics

The TJ-II is equipped with a wide range of passive and active plasma diagnostics [28]. Diagnostics that are of particular relevance include a Thomson Scattering (TS) system that

provides one set of electron density and temperature profiles per discharge [29], as well as a microwave interferometer and an 11 channel Electron Cyclotron Emission (ECE) system that follow the line-integrated electron density and the electron temperature evolution at different radii, respectively, along a discharge. Note: the TS laser chord traverses completely the plasma, hence providing profiles of two poloidal regions (usually named $\rho \geq 0$ and $\rho < 0$); however for TS electron density profiles used here, data from $\rho \geq 0$ are considered due to a signal contamination problem for $\rho < 0$. These systems are located at 180º, 67.5º and 123.75º toroidally, respectively, from the PI. See Figure 2. Note: the microwave-based diagnostics have 10 μs temporal resolution. Finally, the majority ion temperature is measured along a discharge using Neutral Particle Analyzers.

4. Experiments

In these experiments, pellets containing between 0.5 and 1.3×10^{19} hydrogen particles are injected into plasmas created using the standard magnetic configuration, 100_44_64, where the nomenclature reflects currents in the central, helical and vertical field coils, respectively, $1.56 \leq \iota/2\pi \leq 1.64$ (ι is rotational transform) and a magnetic field gradient of -0.9 T/m. For these, plasmas are created and/or maintained with on/off-axis ECRH or by NBI heating. In order to determine pellet particle deposition across the plasma minor radius, and the subsequent radial evolution with time, the shot-to-shot technique is employed where pellets are injected into reproducible plasmas and single TS measurements are made before, during and at several moments after pellet injection. Then, estimating the initial pellet particle content from its mass (obtained with the calibrated PI microwave cavity), the fuelling efficiency is determined from the increase in plasma electron content. For this, the former is obtained using the mass of a hydrogen atom (1.673×10^{-27} kg) while assuming that the density of solid hydrogen is 88 kg/m^3 and pellet mass loss between the microwave cavity and plasma edge is negligible due to the relatively short length (~1.1 m) of the straight guide tubes. Next,

the latter is obtained by integrating the TS electron density profile over the whole plasma volume, assuming an average plasma minor radius of 0.1925 m for the 100_44_64 configuration [30]. As a cross calibration check, the line-averaged density is estimated from a pre-injection TS electron density profile and compared with the corresponding measured microwave interferometer value.

4.1 Pellet Ablation and Plasma Response

In a previous work it was outlined how a pellet ablation profile is established from the recorded Balmer H_α (λ = 656.3 nm) light, emitted by the cold neutral cloud that surrounds the pellet as it traverses the plasma [13]. Here, in Figure 3a, the Hα light fluxes incident on the SIDE and TOP viewports (of Figure 1) are plotted as a function of distance into the plasma for a *Type*-2 pellet injected into an NBI-heated plasma. For this the timing is obtained from the in-line light-gate and microwave cavity diagnostic signals. It is apparent that ablation becomes significant only after a pellet penetrates several centimetres into the plasma and that structures in the profiles, occurring mainly in the core, are reproducible and therefore real. In this example, where the nearest approach to the plasma centre is ρ = 0.273, there are no significant rational surfaces in the core so these striations can be attributed to repeated neutral cloud losses [31]. In addition, when diode light profiles are compared with fast-frame camera images pellet acceleration is not detected parallel to the injection direction. However, toroidal deflections are observed when unbalanced NBI heating is employed [32].

In Ref. [13], it was also described how a T_e profile, as provided by the TS system located 180º toroidally, is perturbed by an inward travelling pellet, *i.e.*, the passing pellet cools the local plasma instantaneously. Note: no inward pre-cooling wave, as reported elsewhere [33], is observed by the ECE diagnostic, albeit in TJ-II such a wave is sometimes observed during TESPEL injections (V_{TESPEL} = ~200 m s^{-1}) [34]. In Figure 3b, it is seen that for NBI-heated plasma the central T_e recovers to pre-injection values within a few milliseconds while the

central ion temperature, T_i, recovers slightly more slowly. In all injections here the percentage drop is ≥15%. In contrast, for ECRH-only plasma, the ensuing T_e is significantly lower than pre-injection values during an extended period and counter mirrors the electron density. See Figure 3c. For this, the microwave power absorption is nearly constant, since reduced absorption due to a fall in electron temperature is counter balancing the increased absorption due to a higher electron density. Moreover, it is seen that T_i increases after pellet injection. This is a consequence of both an increase in N_e and a reduction in T_e, since collisional coupling with the electrons is the only energy source to the ions, and it scales roughly with $N_e^2 T_e^{-1/2}$ for $T_e >> T_i$.

Next, in Figure 4, H_α light profiles emitted by reproducible pellets injected into reproducible ECRH and NBI-heated plasmas highlight the reliability of the shot-to-shot technique for pellet studies in TJ-II. Moreover, in the case of ECRH, they evince that suprathermal electrons, normally located near the plasma edge, do not enhance ablation. Note: for the standard TJ-II configuration electrons with energies ≥70 keV are confined between $0.67 \leq |\rho| \leq 0.9$ [35, 36] where they circulate in a counter-clockwise direction in Figure 2. In contrast, for plasmas created and maintained by NBI heating only, core localized fast electrons, generated during field ramp-up in this unconventional operation mode, can sometimes persist along a discharge and trigger enhanced ablation, as is seen in discharge #37984 of Figure 4. Here, the plasma currents are ~-2.82 kA and ~0.23 kA at pellet injection for discharges #37984 and #38055, respectively. In the same figures, assuming that H_α emissions are proportional to pellet ablation rates [37], then reasonable agreement is found between H_α emissions and modelled ablation curves. These curves were created using Neutral Gas Shielding (NGS) based modelling codes [18, 38], the latter considering fast ion as well as electron impacts. In both cases experimental TS target T_e and N_e profiles are employed.

4.2 Pellet particle deposition and efficiency

It is observed here that the evolution of the pellet electron distribution around the plasma is significantly slower than the thermal perturbation, *i.e.*, it requires several milliseconds to achieve complete particle distribution. Thus in order to determine pellet fuelling efficiency it is necessary to follow the electron density for several ms after pellet injection and in this way identify a maximum.

4.2.1 ECRH plasmas

In Figure 5a, the evolution of the electron density profile during several ms after injection, and the resultant net increase in electron density, is shown for the pellet injections of Figure 4a. This time embodies the complete ionization of the neutral gas cloud that surrounds the pellet and the subsequent transport of particles about the plasma volume. Here, by integrating these profiles over the whole plasma volume, assuming that the electron density is a flux-constant, the temporal evolution of the pellet particle population in the plasma is determined. See Figure 5b, in which the initial pellet particle deposition profile is well reflected by the reconstructed H_α profile, albeit with a small ΔR offset. It should be noted that the increased $H\alpha$ signal that occurs inside $\rho = 0.15$, when the pellet is almost completely ablated, may be due to plasma current, ~0.43 kA. It is postulated that fast electrons continue to reside at, or near, the plasma centre due to lower plasma resistivity, giving rise to increased H_a emission from the neutral cloud. Next, in Figure 6, the maximum deposited pellet electron population occurs ~4 ms after pellet entry, this being followed by a slow decay. When compared with line-averaged electron density evolution, the slower decay of the former is accounted for by a higher weighting of particles deposited in the core to the line-averaged density. Finally, comparing net electron gain by the plasma with pellet particle content, a value of ~36% for fuelling efficiency is obtained for the injections depicted in Figures 4a & 5 (at 3.9 ms). Note: contributions to the density increase due to possible increased neutral recycling caused by a

plasma edge temperature drop are considered negligible, as such fuelling is minimal for the short time window involved.

4.2.2 NBI plasmas

A representative injection for NBI heated plasmas is presented in Figure 7. For such plasmas, the target T_e's and N_e's are significantly lower and higher, respectively, with respect to ECRH, while after an injection T_e is seen to recover its pre-injection value within a few milliseconds. See Figure 3. In addition, as for ECRH, the initial particle deposition of the *Type*-2 pellet in Figure 7 is very similar to its reconstructed H_α profile. Here ΔR is less than 2 cm. Moreover, subsequent partial inward transport leads to an increased core electron density at 18.7 ms [14]. Treating the data in Figure 7 as previously, a pellet fuelling efficiency of ~34% (for 2.7 ms) is determined here for a target $N_e(0) = 10^{19}$ m^{-3}. Note: compared to the pellet fuelling, the NBI contribution is no more than a few percent for this same time interval. Additional injections were made with *Type*-2 pellets into a range of NBI-heated plasmas having a broad range of target densities and the resultant fuelling efficiencies are plotted in Figure 8. It is apparent that fuelling efficiency improves with increasing target density (analogous to decreasing electron temperature), a finding that is consistent with that reported in Ref. [10]. Here, uncertainty in pellet mass due to microwave cavity signal noise is the main contributor to the error bars. Finally, it should be noted that when larger *Type*-3 pellets are employed a significant fraction of the pellet remains and exits the plasma on the high-field side thereby leading to a reduced efficiency.

Measured and predicted plasma energy losses due to pellet injection can be compared to determine if all particles are ablated and ionized by the plasma. For instance, in Figure 3b, a T*ype*-2 pellet (7.7×10^{18} H) and a *Type*-3 pellet (1.42×10^{19} H) are injected into plasma having line-averaged densities of ~1.3×10^{19} m^{-3} and ~1.45×10^{19} m^{-3}, respectively. Then, assuming 36.4 eV loss per ion pair due to ablation, dissociation, *etc*. [39], the plasma energy losses

(26+/-5 J and 48+/-4 J of Figure 3b) measured with diamagnetic loops [26] agree reasonably with predicted losses (22.4 J and 40.8 J, respectively). Here $E_{loss} = (N_H/2) \times 36.4 \times 1.6\times10^{-19}$, where N_H is the number of hydrogen atoms in a pellet. It is assumed that radiation losses are <1 eV/H atom and that plasma dilution by pellet electrons is slow compared with this fast measurement (several ms compared with ~200 μs). This would indicate that pellet injection and associated processes are mainly adiabatic. It would also indicate that pellets arrive intact at the plasma, hence a fast outward drift may be causing the near instantaneous pellet particle loss from the plasma.

5. Conclusions

A cryogenic pellet is now fully operational on the stellarator TJ-II. Associated diagnostics have been tested and have been shown to provide pellet mass, velocity and arrival times as well as ablation and deposited particle profiles. In addition, pellet mass and velocity reproducibility have been demonstrated and allow pellet diffusion and efficiency studies to be made. In the studies performed to date, enhanced ablation due to suprathermal electron populations at the edge of ECRH plasmas is not observed. Instead, rather good agreement is found between experimental and modelled H_α ablation profiles. Moreover, when compared with deposited pellet electron profiles, there is no strong evidence for a significant radial offset between ablation and deposition profiles as is commonly reported for LFS injections and associated with an E×B drift. However, when performing pellet particle accountability for LFS injections, the relatively low efficiencies measured indicate significant pellet particle loss during the ablation process. It is assumed that mass loss due to kinetic friction between a pellet and the straight guide-tube walls (after passing through the microwave cavity) is minimal. In the future, given the flexibility of the TJ-II, complementary studies will be performed for a broad range of magnetic configurations, for example, a scan of iota profile or magnetic well.

Acknowledgements

This work has been carried out within the framework of the EUROfusion Consortium and has received funding from the Euratom research and training programme 2014-2018 under grant agreement No 633053. The views and opinions expressed herein do not necessarily reflect those of the European Commission. In addition, it is partially financed by grants from the Spanish Ministerio de Ciencia y Innovación (Refs. ENE2013-48679-R and ENE2015-70142-P). The authors thank the TJ-II team for their assistance with the work.

References

[1] L. R. Baylor, *et al*., Nucl. Fusion **47** (2007) 443.

[2] F. Warmer, C. D. Beidler, A. Dinklage, R. Wolf and The W7-X Team, Plasma Phys. Control. Fusion **58** (2016) 074006.

[3] H. Maaßberg, C. D. Beidler, and E. E. Simmet, Plasma Phys. Control. Fusion **41** (1999) 1135.

[4] M. Z. Tokar, Nucl. Fusion **23** (1983) 1395.

[5] Y. Lianghua and J. Baldzuhn, Plasma Sci. Tech. **5** (2003) 1933.

[6] E. Speth, Rep. Prog. Phys. **52** (1989) 57.

[7] S. K. Combs, Rev. Sci. Instrum. **64** (1993) 1679.

[8] S. L. Milora, W. A. Houlberg, L. L. Lengyel and V. Mertens, Nucl. Fusion **35** (1995) 657.

[9] B. Pégourié, Plasma Phys. Control. Fusion **49** (2007) R87.

[10] J. Baldzuhn, L. R. Baylor, J. F. Lyon and W7-AS team, Fusion Sci. Tech. **46** (2004) 348.

[11] H. Yamada *et al*, Fusion Eng. Des. **49-50** (2000) 915.

[12] R. Sakamoto *et al*., Nucl. Fusion **46** (2006) 884.

[13] K. J. McCarthy, *et al*., 1st EPS Conference on Plasma Diagnostics, *Frascati*, *Italy*, Proc. of Science (ECPD2015) 134.

[14] J. L. Velasco *et al*., Plasma Phys. Control. Fusion **58** (2016) 084004.

[15] J. A. Alonso *et al*., sent for publication to Phys. Rev. Lett.

[16] J. A. Alonso *et al*., Plasma Phys. Control. Fusion **58** (2016) 074009.

[17] Y. Turkin *et al*., Joint 19th ISHW and 16th IEA-RFP Workshop (2013, Padua, Italy), http://www.igi.cnr.it/ish_rfp_ws2013/content/programme.

[18] P. B. Parks and R. J. Turnbull, Phys. Fluids **21** (1978) 1735.

[19] P. B. Parks, W. D. Sessions, and L R. Baylor, Phys. Plasmas **7** (2000) 1968.

[20] P.T. Lang *et al*., Phys. Rev. Lett. **79** (1997) 1487.

[21] S.K. Combs *et al*., Fusion Tech. **34** (1998) 419.

[22] R. Sakamoto *et al*., Nucl. Fusion 44 (2004) 624.

[23] J. Sánchez *et al*., Nucl. Fusion **55** (2015) 104014.

[24] F. L. Tabarés *et al*., Contrib. Plasma Phys. **50** (2010) 610.

[25] S. K. Combs et al., Fusion Sci. Tech. **64** (2013) 513.

[26] K. J. McCarthy, *Diagnostic tools for probing hot magnetically confined plasmas*, XXXIII Reunión Bienal de la Real Sociedad Española de Física: 21er Encuentro Ibérico para la Enseñanza de la Física: PUBliCan, ediciones de la Universidad de Cantabria, Santander, Spain, **IV** (2011) 65. ISBN 978-84-86116-40-8.

[27] J. Herranz, F. Castejón, I. Pastor and K J. McCarthy, Fusion Eng. Des. **65** (2003) 525.

[28] L. Pacios *et al*., Proc. 11th IEEE NPSS Conf. (Santa Fe, 1999) 243.

[29] F. Tabares *et al*., 32nd EPS Conference on Plasma Phys. (Tarragona, Spain) ECA Vol. **29C**, P-4.008 (2005).

[30] A. Lopez Fraguas, private communication.

[31] P. B. Parks, Plasma Phys. Control. Fusion 38 (1996) 571.

[32] N. Panadero *et al*., 43rd EPS Conference on Plasma Phys. (Leuven, Belgium) ECA Vol. **40A**, P1.008 (2016).

[33] L. Ledl *et al*., Nucl. Fusion **44** (2004) 600.

[34] N. Tamura *et al*., Rev. Sci. Instrum. **87** (2016) 11D619.

[35] P. Medina, *et al*., Rev. Sci. Instrum. **72** (2001) 471.

[36] M. A. Ochando, F. Medina, and TJ-II Team, Plasma Phys. Control. Fusion **45** (2003) 221.

[37] D. H. McNeill, J. Nucl. Mat. **162-164** (1989) 476.

[38] M. Yokoyama *et al*., Nucl. Fusion **47** (2007) 1213.

[39] F. S. Febler *et al*., Nucl. Fusion **19** (1979) 1061.

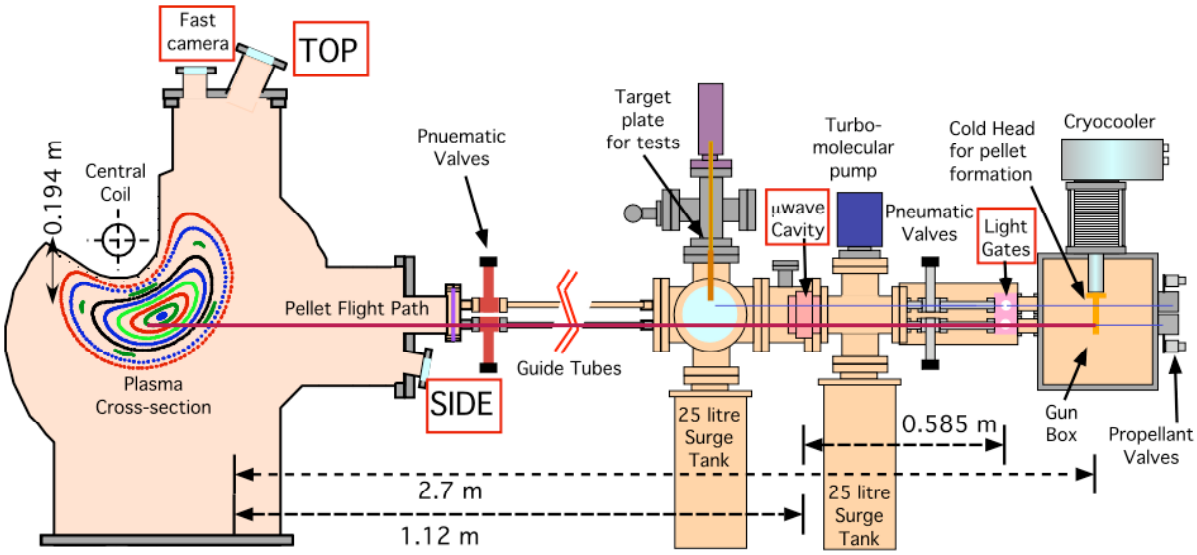

Figure 1. Sketch of the cross-section of the TJ-II and the pellet injector.

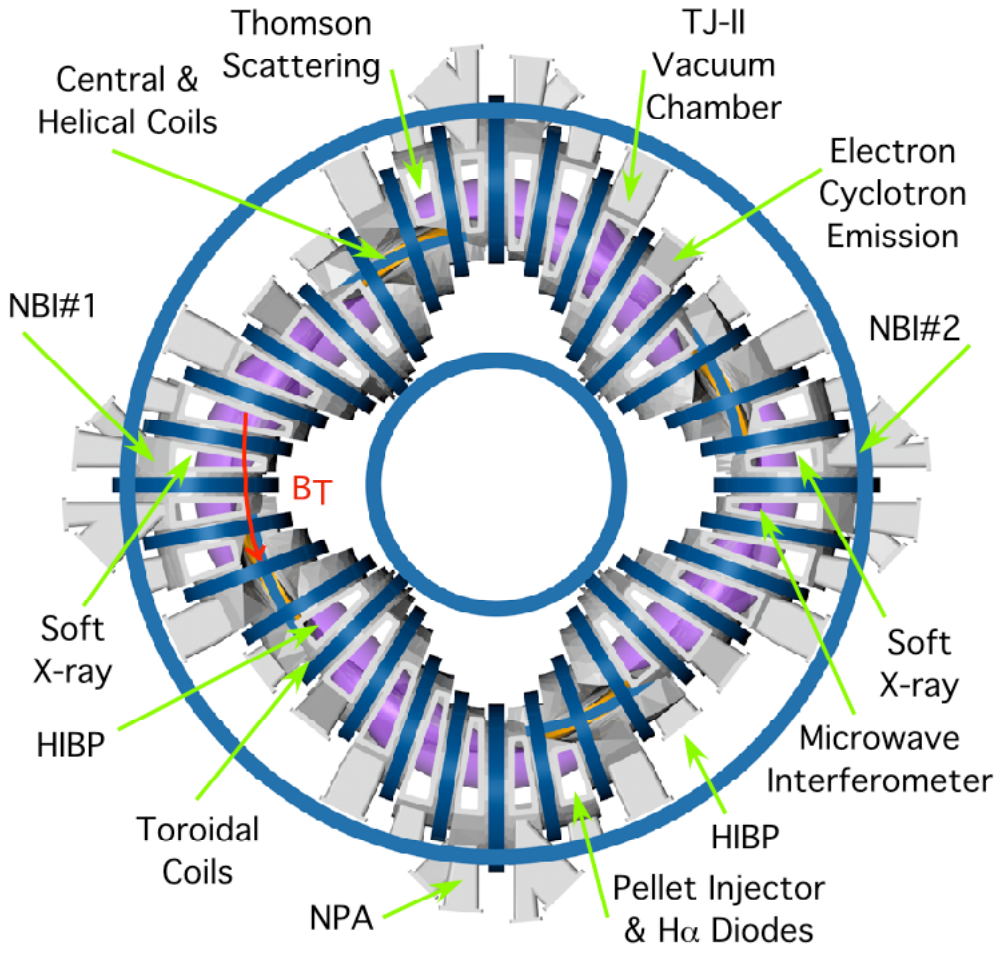

Figure 2. Bird's eye view sketch of the stellarator TJ-II showing the locations of its principal systems and diagnostics.

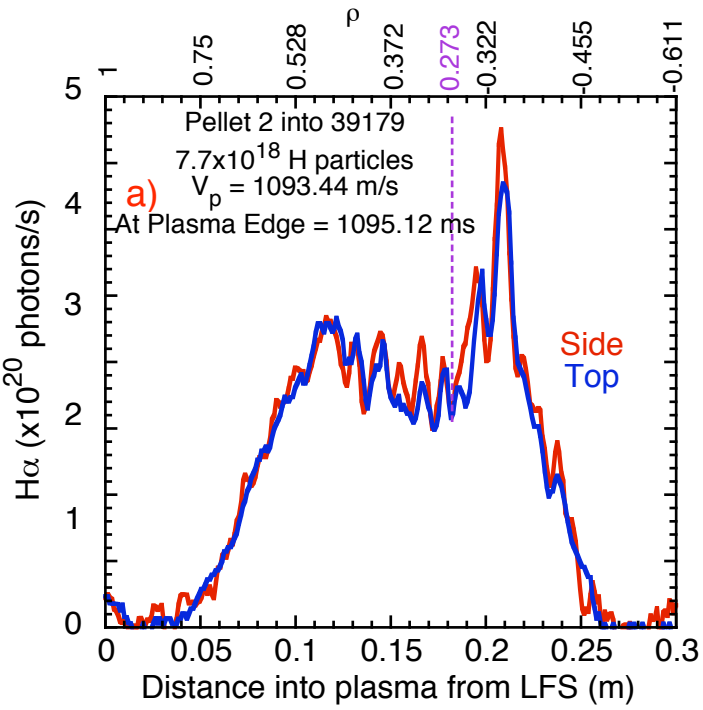
ρ
1
0.75
0.528
0.372
0.273
0.322
0.455
0.611
Pellet 2 into 39179
7.7x10^18 H particles
V_p = 1093.44 m/s
a)
At Plasma Edge = 1095.12 ms
Side
Top
Hα (x10^20 photons/s)
Distance into plasma from LFS (m)

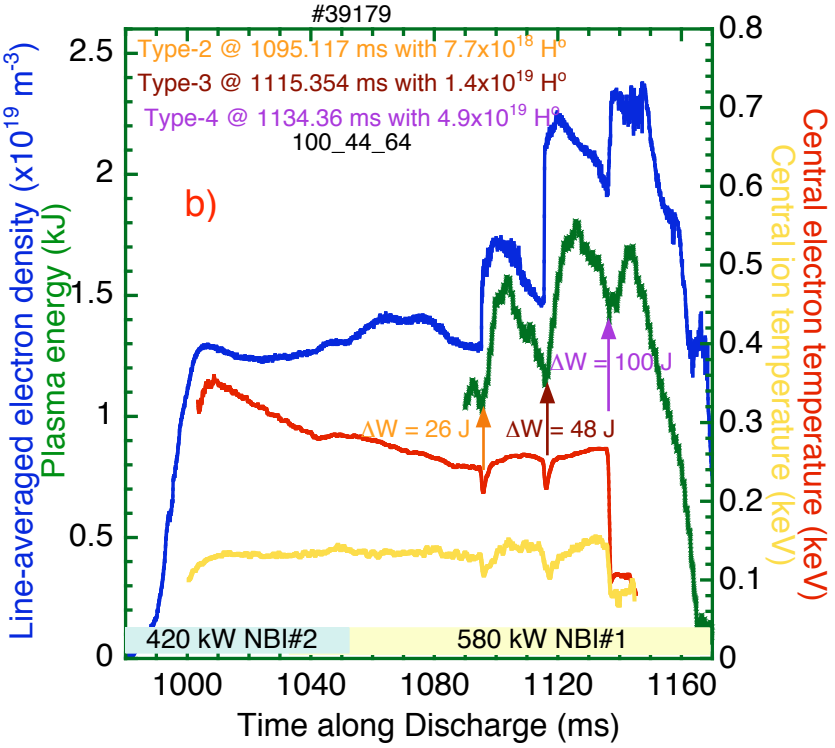
#39179
Type-2 @ 1095.117 ms with 7.7x10^18 H°
Type-3 @ 1115.354 ms with 1.4x10^19 H°
Type-4 @ 1134.36 ms with 4.9x10^19 H°
100_44_64
b)
ΔW = 100 J
ΔW = 26 J
ΔW = 48 J
420 kW NBI#2
580 kW NBI#1
Line-averaged electron density (x10^19 m^-3)
Plasma energy (kJ)
Central ion temperature (keV)
Central electron temperature (keV)
Time along Discharge (ms)

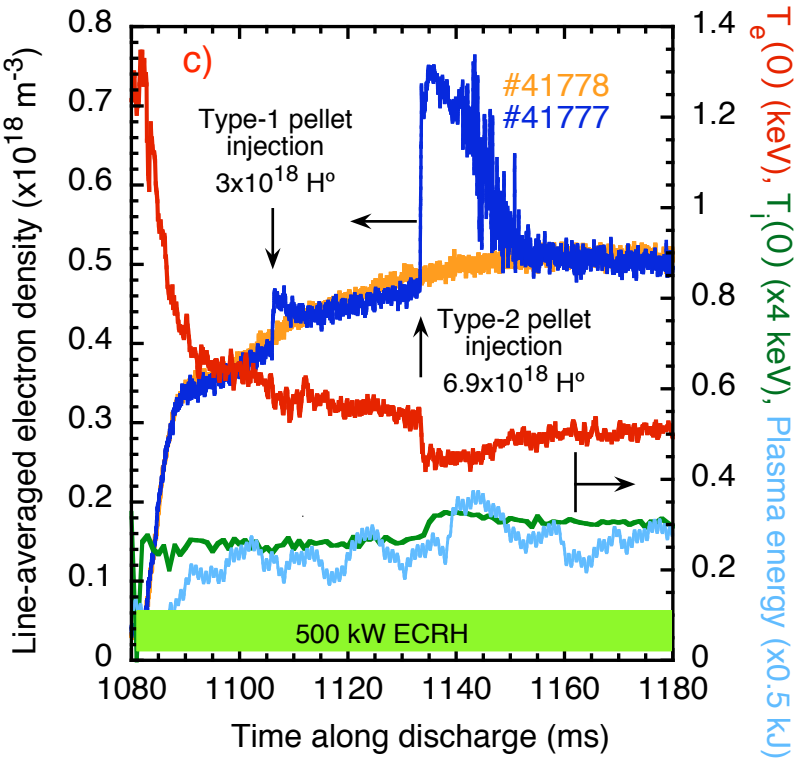

Figure 3: Evolution of a) line-averaged electron density, central electron & ion temperatures, and plasma energy along reproducible ECRH discharges with/without pellet injection, b) plasma parameters along an NBI heated plasma with sequential pellet injections (the largest causes cooling) and c) Hα light intensities incident on Side APD (smoothed) and Top photodiode versus distance into plasma/normalized plasma radius for Type-2 pellet into discharge #37179. Note: ΔW is measured plasma energy loss.

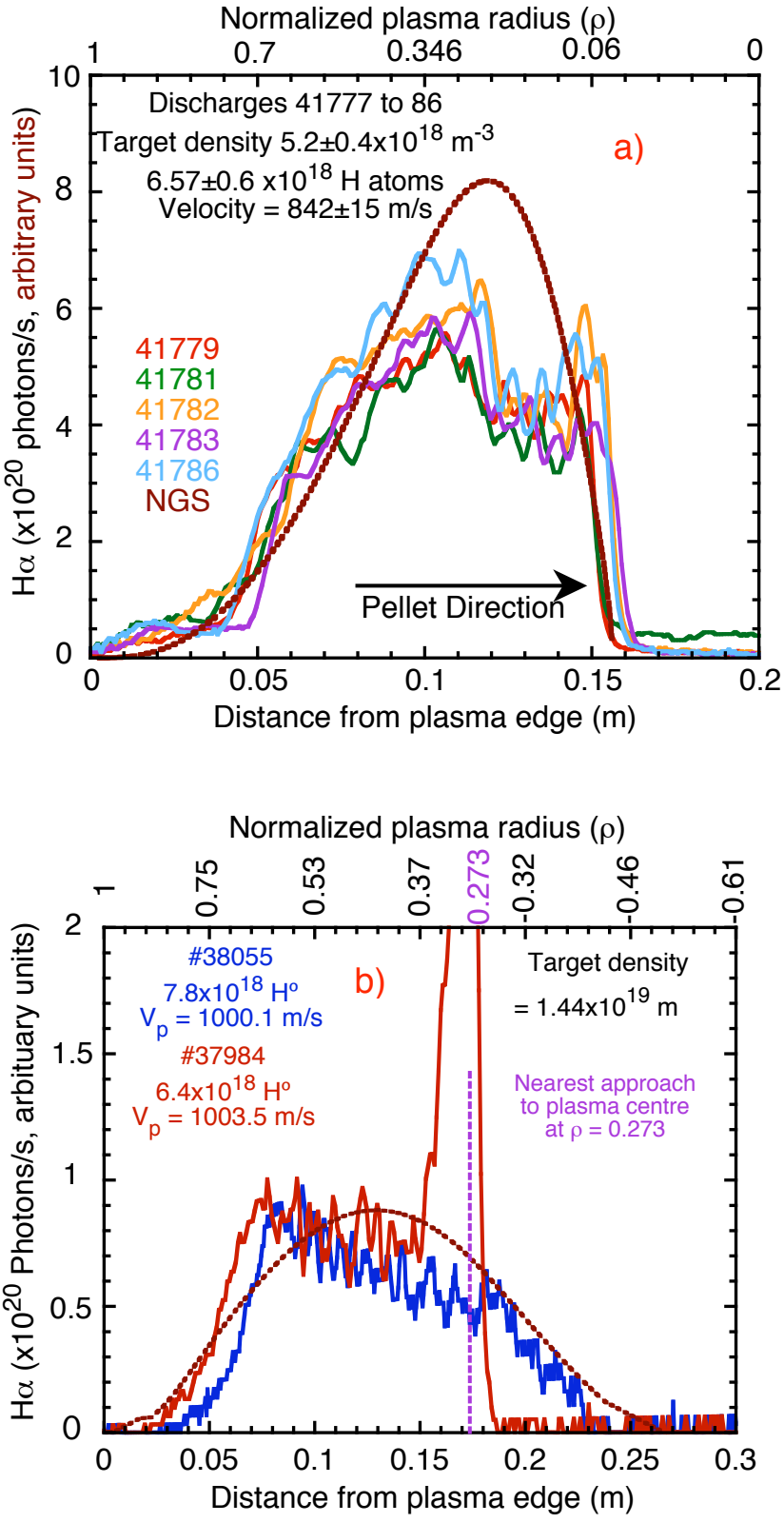

Figure 4: H_α emissions by similar pellets injected into reproducible a) ECRH plasmas and b) NBI-heated plasmas of TJ-II. NGS modelled ablation profiles are shown for representative cases. Note: complete pellet ablation occurs within ~200 μs.

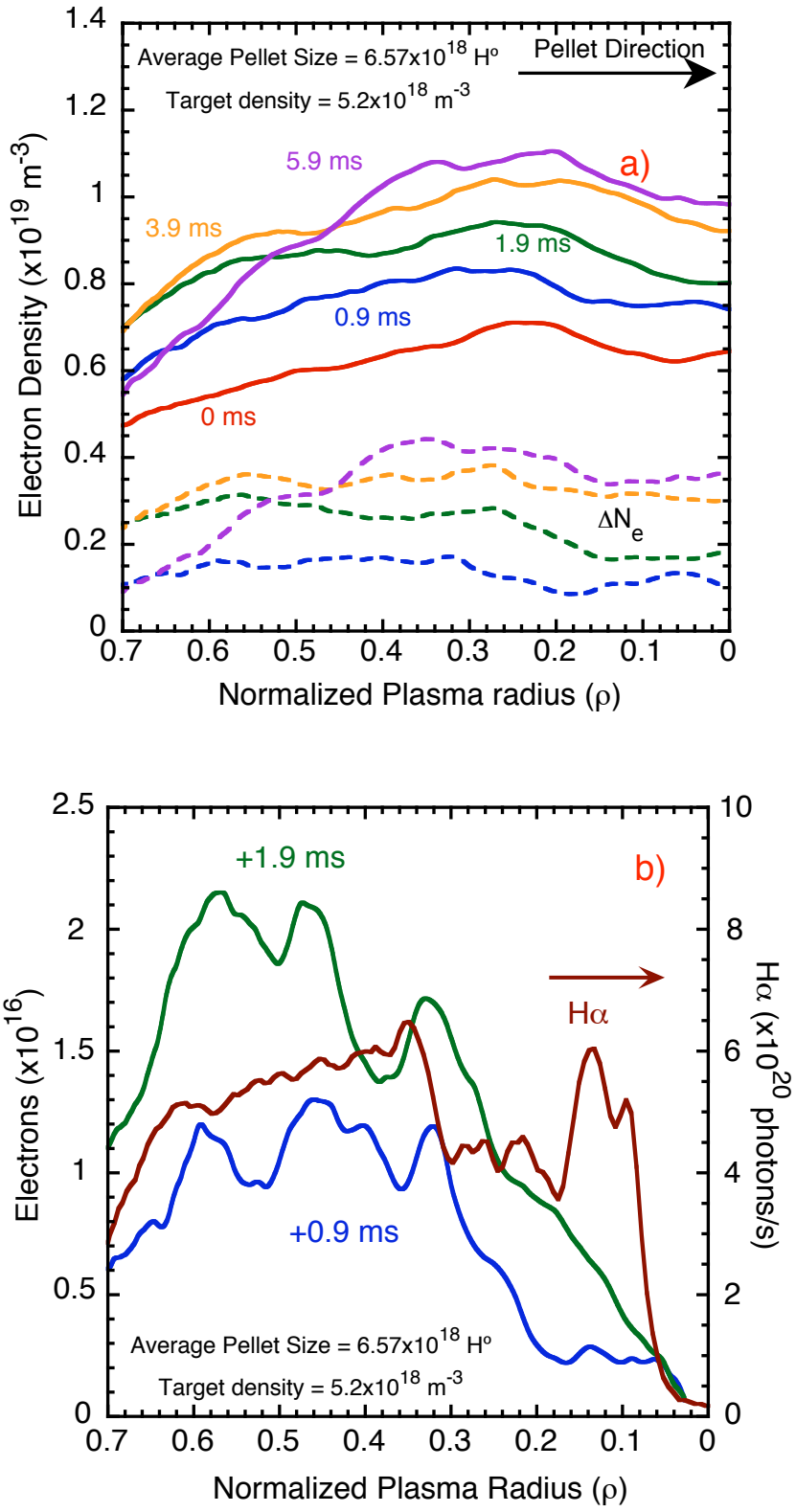

Figure 5. a) Plasma electron density profiles (continuous lines) obtained with the TS system before (red, 0 ms), and at several time points after, pellet injection. Also shown are profiles of the net increase in electron density for the same time points. b) H_α light emitted from the

neutral gas cloud surrounding a pellet and deposited electron distributions after 0.9 ms and 1.9 ms as determined from a).

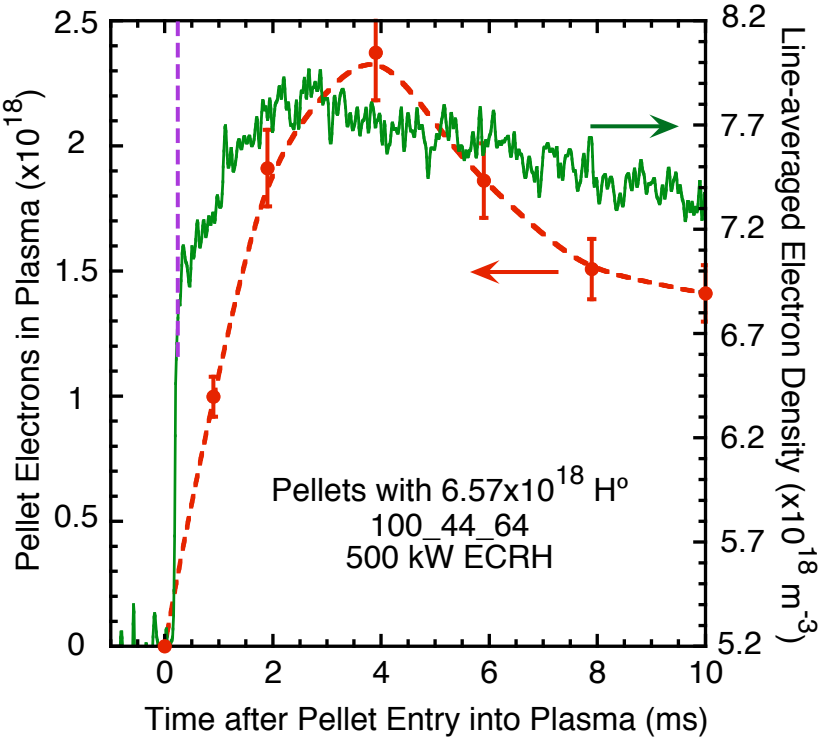

Figure 6: Evolution of plasma pellet electron population (points) and plasma line-averaged electron density (continuous) for reproducible pellet injections into ECRH plasmas of Figure 4a. Note: the dashed red line is used to guide the eye. The line-averaged density of the target plasma is 5.2×10^{18} m^{-3}. Small corrections have been made for shot-to-shot variations in pellet mass (<5%). Pellet are fully ablated ~200 μs after plasma entry (vertical dashed).

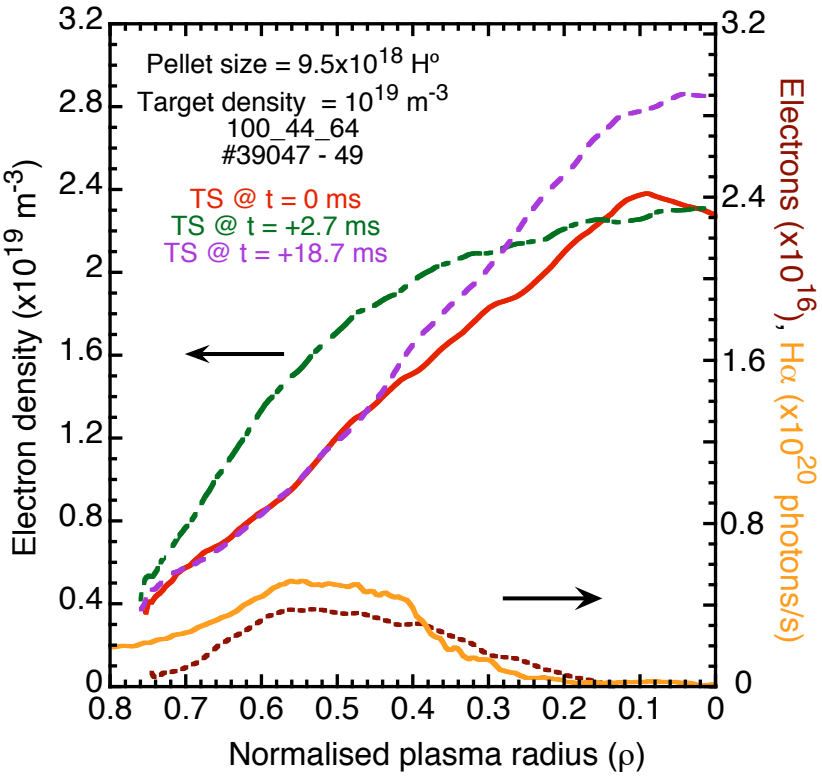

Figure 7: Evolution of electron density profile before (continuous), and at two time steps (dot-dash for 2.7 ms and dash for 18.7 ms) after, pellet injection into an NBI heated plasma created with the standard magnetic configuration. Also, shown are deposited electron (dot for 2.7 ms) and H_α emission (continuous) profiles.

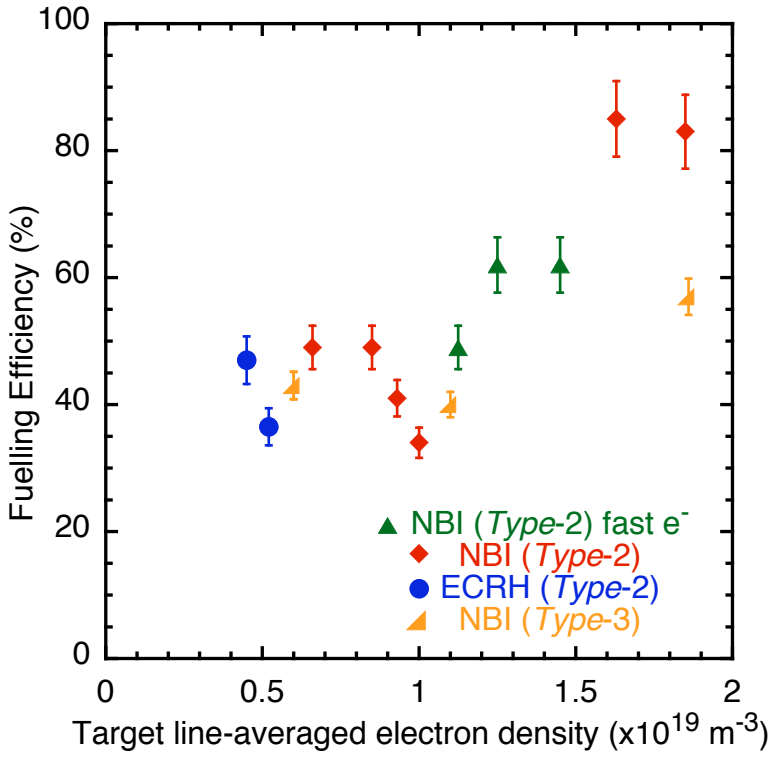

Figure 8: Pellet fuelling efficiency versus target line-averaged electron density for ECRH and NBI heated plasmas created using the standard TJ-II magnetic configuration.